Available online at www.sciencedirect.com
ScienceDirect
Inorganica Chimica Acta 361 (2008) 2747–2758
Inorganica Chimica Acta
www.elsevier.com/locate/ica

New dinuclear cobalt(II) octaaza macrocyclic complexes with high oxidation redox potentials: Their crystal structure and unusual magnetic properties

Jayanthi Narayanan [a], Alejandro Solano-Peralta [a], Víctor Manuel Ugalde-Saldivar [a], Roberto Escudero [b], Herbert Höpfl [c], Martha Elena Sosa-Torres [a,*]

[a] *División de Estudios de Posgrado, Facultad de Química, Universidad Nacional Autónoma de México, Cd. Universitaria, 04510 México DF, México*
[b] *Instituto de Investigaciones en Materiales, Universidad Nacional Autónoma de México, Cd. Universitaria, 04510 México DF, México*
[c] *Centro de Investigaciones Químicas, Universidad Autónoma del Estado de Morelos, Ave. Universidad 1001, Cuernavaca, 62209 Morelos, México*

Received 1 December 2007; accepted 29 January 2008
Available online 13 February 2008

Abstract

Dinuclear cobalt(II) complexes were synthesised from 1,4,8,11-tetrakis-(2-pyridylmethyl)-1,4,8,11-tetraazacyclotetradecane (*tmpc*), $[Co_2(tmpc)Cl_2][CoCl_4]$ (**1**), $[Co_2(tmpc)Cl_2][PF_6]_2$ (**1a**) and $[Co_2(tmpc)(NO_3)_2][NO_3]_2 \cdot MeOH$ (**2**) and characterised by magnetic, spectroscopic and electrochemical techniques and by single-crystal X-ray diffraction. The X-ray structures of **1** and **2** demonstrate that in both complexes the metal ion is *exo*-coordinated with respect to the macrocyclic ligand. In **1**, the Co(II) ions are fivefold coordinated with trigonal bipyramidal geometry, while in **2** they are sixfold coordinated with a distorted octahedral geometry. The high magnetic moments obtained for these complexes are explained in terms of a *spin–orbit* coupling. Magnetic measurements show a deviation from the Curie–Weiss law at low temperatures. Two magnetic orderings were observed, at high temperatures an antiferromagnetic coupling was found, below 20 K a change to a weak ferromagnetic coupling was observed. Isothermal magnetic measurements at low temperature show a weak hysteresis, which was confirmed by the small coercive field found at low temperature. In addition, for the first time an explanation for the observation that these cobalt(II) compounds are very stable towards oxidation is offered in terms of the high redox potential values obtained for **1**, **1a**, and **2**.

Keywords: High spin dinuclear cobalt(II); X-ray diffraction; Pentacoordination; *exo*-Coordination of *N*-substituted macrocyclic ligand; Magnetic properties; EPR and electrochemistry

1. Introduction

The pyridyl substitution of nitrogen atoms in tetraazamacrocyclic compounds has been shown to stabilise the lower oxidation states of transition metal compounds [1]. The modification of tetraazamacrocyclic ligands to control and tune the redox properties of coordinated metal centres has been the subject of continuing interest. Variations can be introduced by altering the size of the macrocyclic ring by placing the substituents on the nitrogen donors and/or on the ring framework [2]. Tetraazamacrocycles having four pendant coordinating groups attached to the four nitrogen atoms have been suggested as ligands for the formation of binuclear metal complexes [3]. Vuckovic et al., have recently reported on binuclear Co(II) and Cu(II) complexes [4] with the ligand 1,4,8,11-tetrakis-(2-methylpyridyl)-1,4,8,11 tetraazacyclotetradecane *tmpc*, Scheme 1, in which each metal ion is coordinated by two cyclam ring nitrogen atoms and two pendant pyridyl nitrogen atoms, additional atoms of the macrocyclic ligands are acting as a bridge between the two metal centres.

* Corresponding author.
E-mail address: mest@servidor.unam.mx (M.E. Sosa-Torres).

0020-1693/$ - see front matter © 2008 Elsevier B.V. All rights reserved.
doi:10.1016/j.ica.2008.01.049

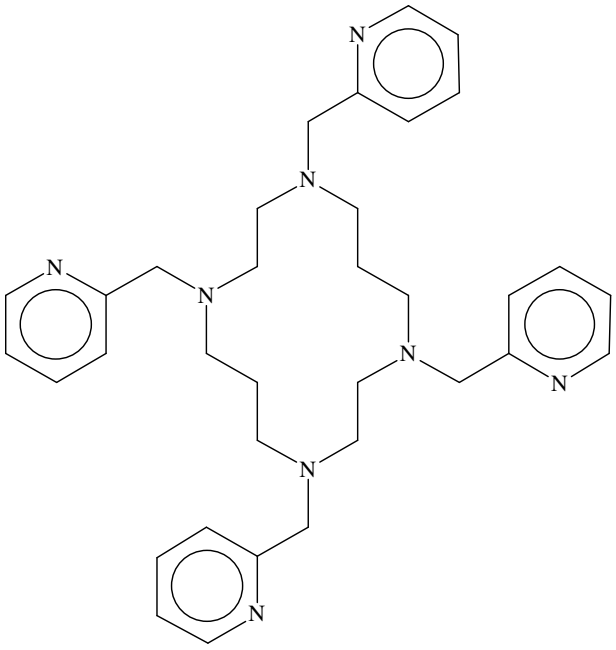

Scheme 1. 1,4,8,11-tetrakis-(2-pyridylmethyl)-1,4,8,11-tetraazacyclotetradecane (*tmpc*) [5].

Alternatively, complexes with high spin d^7 configuration are of great interest since they might exhibit interesting magnetic properties. Thus, because of our interest in exploring the intrinsic properties that influence the electronic configuration on the dinuclear hs Co(II) complexes, a complete study of $[Co_2(tmpc)Cl_2][CoCl_4]$ (**1**), $[Co_2(tmpc)Cl_2][PF_6]_2$ (**1a**) and $[Co_2(tmpc)(NO_3)_2][NO_3]_2 \cdot MeOH$ (**2**) was carried out. This includes the synthesis and characterisation by spectroscopic, magnetic and electrochemical studies. Moreover, the crystal and molecular structures of **1** and **2** are reported. The results obtained offer an explanation for the reason why this ligand can stabilise the cobalt ions in low oxidation states.

2. Experimental

2.1. Materials and methods

All reagents were purchased from Aldrich Chemical Co. Solvents were dried according to procedures reported in the literature.

Elemental analyses for C, H and N were carried out using a Fisons instrument microanalyzer model EA 1108 at the USAI – Facultad de Química, UNAM, México.

Fourier transformed infrared spectra on KBr pellets in the range of 4000–450 cm^{-1} were recorded on a Perkin–Elmer/1600 FT IR instrument, while in the range of 700–100 cm^{-1} were recorded on a NICOLET/740 FT IR spectrophotometer.

Electronic absorption spectra were measured on a Hewlett–Packard 8452 Diode Array spectrophotometer, and diffuse reflectance spectra were recorded on a Cary 5E UV/Vis/NIR instrument.

EPR spectra were recorded on polycrystalline samples with a Bruker Elexsys E500 spectrometer using the X-band (9.45 GHz) microwave frequency operating at 100 kHz. The X-band EPR at low temperature was performed with an Oxford liquid helium continuous flow cryostat. The *g*-values were determined by measuring the magnetic field *H* and the microwave frequency.

The magnetic susceptibility measurements were obtained by using the Gouy balance at 300 K which was calibrated with $Hg[Co(SCN)_4]$ as standard. The effective magnetic moments were calculated from the expression: $\mu_{eff} = 2.83\sqrt{\chi_{Mcd} \cdot T}$ BM. Magnetization versus temperature was measured in the presence of 1000 Oe from 2 to 300 K and carried out using a MPMS SQUID magnetometer. Isothermal magnetization studies as a function of field strength (0–10000 Oe) were made at several temperatures. All magnetic measurements were performed on microcrystalline powdered samples and corrected for the diamagnetic contribution using Pascal's constants. The value of 140×10^{-6} cm^3 mol^{-1} was used as the temperature-independent paramagnetism (Nα) of Co(II) ion.

The voltammetric measurements were carried out on an EG&G Potentiostat–Galvanostat model PAR 273-A, using a three-electrode potentiostatic system in acetonitrile containing 0.10 M Bu_4NPF_6 as a supporting electrolyte in each case and were carried out with a glass carbon electrode (surface area 7.1 mm^2), Ag^0–AgCl as a reference electrode and platinum wire as a counter electrode. The ferrocene–ferrocenium couple served as an internal reference, potentials being given in V referred to ferrocene–ferrocenium ($E_{1/2} = 0.685$ V/Ag–AgCl). Cyclic voltammograms of the *tmpc*, $CoCl_2 \cdot 6H_2O$ and *t*-butylammonium chloride were also performed.

2.2. Synthesis of ligand 1,4,8,11-bis(tetramethylphenyl)-1,4,8,11-tetraazatetracyclodecane (tmpc)

This ligand was prepared as previously published. *Anal.* Calc. for $C_{34}H_{44}N_8$: C, 72.30; H, 7.84; N, 19.84. Found: C, 72.46; H, 8.11; N, 20.02% [6].

2.3. Synthesis of $[Co_2(tmpc)Cl_2][CoCl_4]$ (1)

The *tpmc* ligand (0.564 g, 1 mmol) was dissolved in ethanol (10 mL at 40 °C) and added to an ethanolic (10 mL at 40 °C) solution of $CoCl_2 \cdot 6H_2O$ (0.714 g, 3 mmol), which was kept under vigorous stirring for 20 min; when room temperature was reached, a blue solid precipitated (0.9 g, 95%). A methanolic solution of this compound was allowed to evaporate slowly until the fine shining deep royal blue crystals suitable for X-ray analysis were obtained. *Anal.* Calc. for $C_{34}H_{44}N_8Co_3Cl_6$: C, 42.79; H, 4.65; N, 11.74. Found: C, 43.26; H, 4.91; N, 11.94%.

2.4. Synthesis of $[Co_2(tmpc)Cl_2][PF_6]_2$ (**1a**)

This compound was obtained from compound **1**. A saturated solution of NH_4PF_6 in methanol was added to a methanolic (10 mL at 40 °C) solution of **1** (0.954 g, 1 mmol). A pale blue solid precipitated and was washed several times with methanol (1.0 g, 98%). *Anal.* Calc. for $C_{34}H_{44}N_8Co_2Cl_2P_2F_{12}$: C, 39.15; H, 4.26; N, 10.75. Found: C, 39.38; H, 4.06; N, 10.24%.

2.5. Synthesis of $[Co_2(tmpc)(NO_3)_2][NO_3]_2 \cdot MeOH$ (**2**)

This compound was prepared as **1**, but by using *tpmc* (0.564 g, 1 mmol) and $Co(NO_3)_2 \cdot 6H_2O$ (0.582 g, 2 mmol) in methanol. A pink crystalline compound was obtained (0.9 g, 97%). This compound was recrystallized from a mixture of methanol and acetonitrile. Bright pink crystals suitable for X-ray analysis were obtained. *Anal.* Calc. for $C_{35}H_{48}N_{12}Co_2O_{13}$: C, 43.67; H, 5.03; N, 17.46. Found: C, 43.64; H, 5.27; N, 17.34%.

2.6. Crystallographic studies

X-ray diffraction studies of single crystals for compounds **1** and **2** were conducted at room temperature on a BRUKER-AXS APEX diffractometer equipped with a CCD area detector ($\lambda_{Mo\,K\alpha} = 0.71073$ Å, monochromator: graphite). Frames were collected via ω/Φ-rotation at 10 s per frame [7]. The measured intensities were reduced to F^2 and corrected for absorption with SADABS [8]. The cell parameters were determined by using reflections from all frames collected. Structure solution, refinement and data output were carried out with the SHELXTL-NT program package [9]. Non-hydrogen atoms were refined anisotropically. Hydrogen atoms were placed in geometrically calculated positions using a riding model. The asymmetric unit of compound **1** contains two independent molecule halves located at crystallographic inversion centres, of which one is partially disordered over two positions (occupation factors: 0.61 and 0.39 for conformer IIA and IIB, respectively). In the case of compound **2** there is only one independent molecule half that is also located at a crystallographic inversion centre.

3. Results and discussion

3.1. Synthesis

The reaction in anhydrous ethanol (**1** and **1a**) and methanol (**2**) between the cobalt salts $CoCl_2 \cdot 6H_2O$, $Co(NO_3)_2 \cdot 6H_2O$ and the *tmpc* ligand gave compounds **1**: $[Co_2(tmpc)Cl_2][CoCl_4]$, **1a**: $[Co_2(tmpc)Cl_2]$ $[PF_6]_2$ and **2**: $[Co_2(tmpc)(NO_3)_2]$ $[(NO_3]_2 \cdot MeOH$. The reactions were repeated several times, always the same products being obtained.

3.2. Infrared spectra

The IR spectrum for **1** shows ν_{max}/cm^{-1} 2858m [$\nu(CH_2)$], 1606vs [$\nu(C{=}N)$] and 1569s [$\nu(C{=}C)$], which agree well with a coordinated *tmpc*. ν_{max}/cm^{-1} 270m (ν_1) and a doublet at 293vs (ν_3), 306vs (ν_3) and 128(ν_4) are assigned to the Co–Cl vibrations of the tetrahedral tetrachlorocobaltate counterion [10]. Compound **1a** shows ν_{max}/cm^{-1} 2885m [$\nu(CH_2)$], 1610vs [$\nu(C{=}N)$] and 1573s [$\nu(C{=}C)$] and free ionic hexafluorophosphate vibrations at 840vs (ν_3). Compound **2** shows ν_{max}/cm^{-1} 2933m [$\nu(CH_2)$], 1606vs [$\nu(C{=}N)$] and 1569s [$\nu(C{=}C)$], which are shifted to higher energy when compared with the free *tmpc* ligand, thus indicating its coordination. Besides, there are bands corresponding to a coordinated nitrate [11] ion that shows ν_{max}/cm^{-1} 1477m, [$\nu_1(A_1)$-NO_3], 1286m [$\nu_5(B_2)$-NO_3], 1021s [$\nu_2(A_1)$-NO_3], 820m, 833s [$\nu_3(A_1)$-NO_3] and 725s [$\nu_6(B_1)$-NO_3]. ν_{max}/cm^{-1}1766m, 1700vw [$\nu(\nu_2+\nu_3)$-NO_3] being diagnostic of the coordinated mode. Thus, the difference between these two frequencies (60–80 cm^{-1}) can tentatively be assigned to an asymmetric chelating bidentate nitrate [12]. It is important to mention that a very strong band centred at 1383 cm^{-1} and normally assigned to ionic nitrates was also observed.

3.3. Electronic spectra

The solid state reflectance spectrum of **1** (Fig. 1) shows the bands that are expected for the transitions corresponding to a d^7 Co(II) high spin species in a trigonal bipyramidal (tbp) geometry (Table 1), see Scheme 2 [13]. Furthermore, the transitions of the counterion of **1**, a d^7 Co(II) tetrahedral (tet) species appear as a multiple absorption in the visible region (λ_{max}/nm 695–631). In an acetonitrile solution, the visible spectrum of **1** in Fig. 2 shows bands that correspond to the Co(II) high spin (tbp) species. The d^7 Co(II) (tet) species from the counterion remains associated in the acetonitrile solution and appears as the typical multiple absorption. It is to be noted that the spectrum of **1** in the solid state is very similar to that obtained

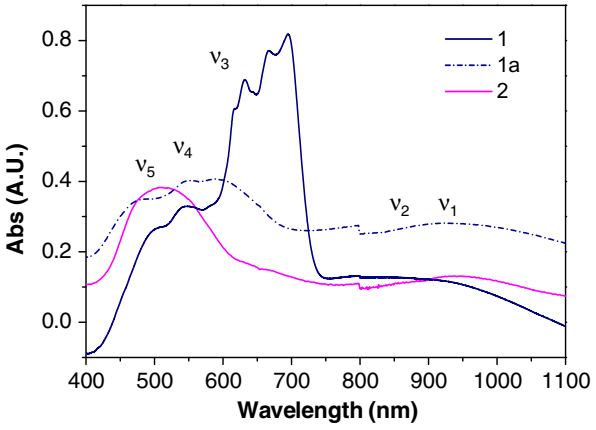

Fig. 1. UV–Vis spectra in the solid state of **1**, **1a** and **2**.

Table 1
Electronic transitions for hs penta-coordinated cobalt(II) complexes **1** and **1a**

	1, λ nm (ε/M^{-1} cm^{-1})			**1a**, λ nm (ε/M^{-1} cm^{-1})	
	Solid	CH_3CN	CH_3OH	Solid	CH_3CN
$^4A_2' \rightarrow {}^4E''$ (P) (ν_5)	500	479 (103)	470 (88)	483	479 (72)
$^4A_2' \rightarrow {}^4A_2'$ (P) (ν_4)	545	543 (124)	550 (110)	552	552 (94)
$^4A_2' \rightarrow {}^4E'$ (F) (ν_3)	615	590 (330)	590 (122)	590	590 (113)
$^4A_2' \rightarrow {}^4E''$ (F) (ν_2), $^4A_2' \rightarrow {}^4A_1'', {}^4A_2''$ (F) (ν_1)	945	963 (58)	960 (20)	933	974 (17)
$CoCl_4^{2-}$	631, 666, 695	626, 650, 682	disappeared		

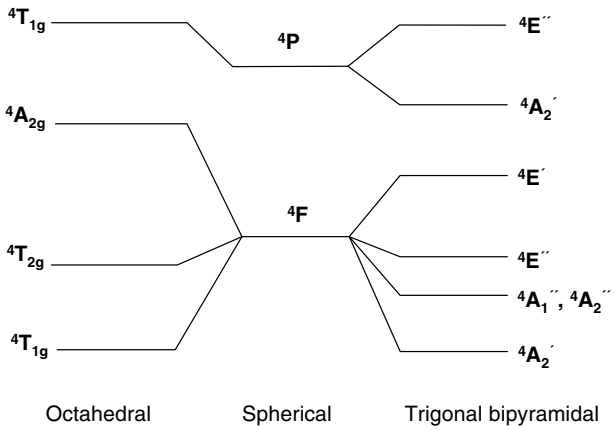

Scheme 2. Energy level diagram for weak octahedral and trigonal bipyramidal fields [13].

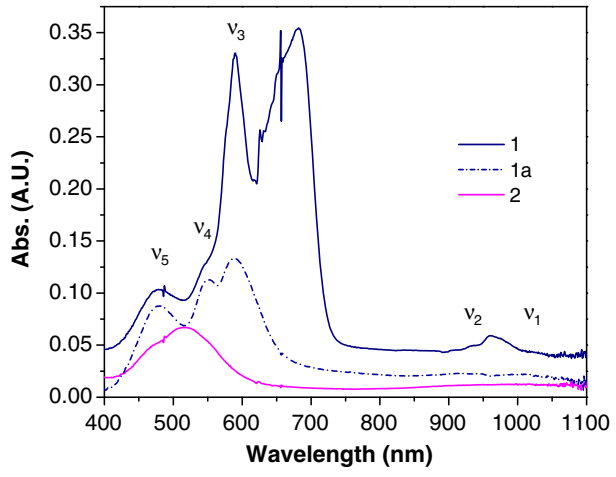

Fig. 2. UV–Vis spectra of **1**, **1a** and **2** in MeCN (1.0×10^{-3} M at 25 °C).

in CH_3CN solution. On the other hand, the transitions that correspond to the cobalt(II) tetrahedral species disappeared when **1** was dissolved in CH_3OH and the transitions corresponding to the tbp species remained, indicating that only the tbp geometry remained in solution.

The solid state reflectance spectrum of **1a** (Fig. 1) shows the corresponding transitions expected for a hs d^7 Co(II) species in a tbp geometry (Table 1). On the other hand, the visible spectrum of **1a** in acetonitrile (Fig. 2) confirms the Co(II) hs, (tbp) species again, since it presents equivalent transitions.

The diffuse reflectance spectrum of **2** shows (Fig. 1) bands that correspond to a d^7 Co(II) high spin species in a octahedral (Oh) geometry, listed in Table 2. The absorption spectrum of **2** in acetonitrile (Fig. 2) and methanol shows equivalent spectra, thus indicating that the Oh geometry is maintained in both solutions.

It can be noticed that the electronic spectra of **1** and **1a** are very similar reflecting the similarities between the two electronic environments of the metals in the trigonal bipyramidal geometry in both complexes, in contrast with **2** which posseses a distorted octahedral geometry.

3.4. Electron paramagnetic resonance

In order to characterise the magnetic Co(II) centres in the penta-coordinated complexes **1**, **1a** and **2**, X-band EPR spectra of polycrystalline samples of the compounds were measured in the temperature range from 4 to 300 K. Though no spectra were observed at room temperature, some started to be seen at 10 K (Fig. 3) as a consequence of the fast spin relaxation time of high spin Co(II). Spectra obtained at 4 K as well as at 10 K for **1**, **1a** and **2** complexes, which were very broad and little resolved without hyperfine splitting, showed a pseudo-rhombic signals with effective g values of: 6.085, 2.415 and 1.153 for **1**; 3.936, 2.118, 1.536 for **1a** and $g = 5.453$, 1.221 and 0.882 for **2**. This large anisotropy is characteristic for cobalt(II) complexes [14].

3.5. Magnetic susceptibility

For **1**, **1a**, and **2**, the determined magnetic moments were μ_{eff}: 8.2, 7.6 and 7.2 BM, respectively. These values are much larger than the *spin* only values for the dinuclear high-spin cobalt(II) (6.7, 5.4 and 5.4 BM, respectively), as determined by $\mu_{SS} = [\sum gi^2 Si\ (Si+1)]^{1/2}$; with $S = 3/2$ for a hs Co(II). The value for **1**, which has three hs cobalt

Table 2
Electronic transitions of the hexacoordinate cobalt(II) complex **2**

	Solid λ_{max}/nm	Solution λ_{max}/nm (ε/M^{-1} cm^{-1})	
		CH_3CN	CH_3OH
$^4T_{1g} \rightarrow {}^4T_{1g}$ (P) (ν_3)	510	472 (50)	460 (73)
$^4T_{1g} \rightarrow {}^4A_{2g}$ (F) (ν_2)	510	515 (67)	540 (99)
$^4T_{1g} \rightarrow {}^4T_{2g}$ (F) (ν_1)	943	1001 (11)	1000 (15)

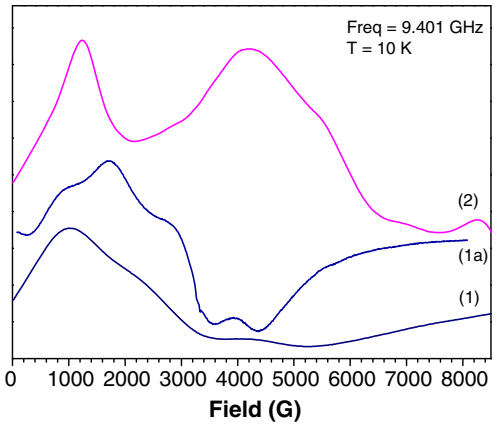

Fig. 3. X-band EPR spectra of microcrystalline samples of **1**, **1a** and **2** at 10 K.

species, is much larger than **1a** and **2**, which has only two hs cobalt species. On the other hand, these values are closer to the expected values, 9.0 and 7.3 and 7.3 BM, if they are calculated considering orbital and spin coupling: $\mu_{LS} = [\sum Li(Li+1) + \sum gi^2 Si(Si+1)]^{1/2}$, where $L = 3$ and $S = 3/2$ [15]. The Co(II) d^7 ion is strongly anisotropic and the first-order orbital momentum is no longer negligible; thus, the found values can be explained by *spin–orbit* coupling. Therefore, we propose that **1**, **1a** and **2** show the contribution of the orbital angular momentum expected for high-spin cobalt(II) species [16,17].

For each compound the magnetic susceptibility as a function of temperature was studied. Fig. 4 displays the inverse of the magnetic susceptibility, χ^{-1}, versus T, for **2**. From room temperature to about 50 K, a clear Curie–Weiss fit showed an antiferromagnetic ordering with a $\Theta_{CW} = -25.09$ K. At lower temperatures, from 50 to 2 K, a deviation from the Curie–Weiss law is observed. Similar magnetic behaviour was observed for **1** and **1a**. The best fit parameters are listed in Table 3.

Fig. 5 shows that the μ_{eff} values decrease as the temperature is lowered to 2 K for the three compounds, this

Table 3
Best-fit parameters of $1/\chi$ vs. temperature (Curie–Weiss law) for **1**, **1a** and **2**

	$T > 50$	
	C (cm^3 K mol^{-1})	θ (K)
1	8.2829	−9.0
1a	7.8690	−20.0
2	6.7691	−25.0

behaviour being consistent with the antiferromagnetic coupling already discussed.

In order to account for intramolecular magnetic interactions, the susceptibility data were analysed by using an isotropic Heisenberg Hamiltonian equation and the results indicate that this intramolecular exchange interaction is negligible.

To investigate other magnetic effects, isothermal magnetic measurements were carried out and the results indicate that **1**, **1a** and **2** possess a hysteretic behaviour (Fig. 6).

This hysteresis is consistent with the observed deviation of the Curie–Weiss law (Fig. 4) since a weak ferromagnetic ordering at low temperatures takes place. On the other hand, the hysteresis for compound **1** measured at 2 K yields a saturation magnetization (M_s) of 0.7 emu, a remanent magnetization (M_r) of 4.00×10^{-4} emu and a coercivity (H_C) of 5.3 Oe, while for **1a** a M_s of 0.51 emu, a M_r of 3.05×10^{-4} emu and $H_C = 5.60$ Oe and finally for **2** there is a hysteresis loop with M_s approaching 0.65 emu, $M_r = 12.10 \times 10^{-4}$ emu and $H_C = 17.5$ Oe at low temperature. These results confirm the weak ferromagnetic coupling between the hs cobalt(II) ions at low temperature. Fig. 7 shows the coercive field for **1** and **2**: H_C which decreases in a linear form, as the temperature is increased. Accordingly, the ferromagnetic coupling disappears at about 16, and 13 K for **1** and **2**, respectively. It is worth noticing that the change in the counterion produced a slight variation in the magnetic response of the complexes.

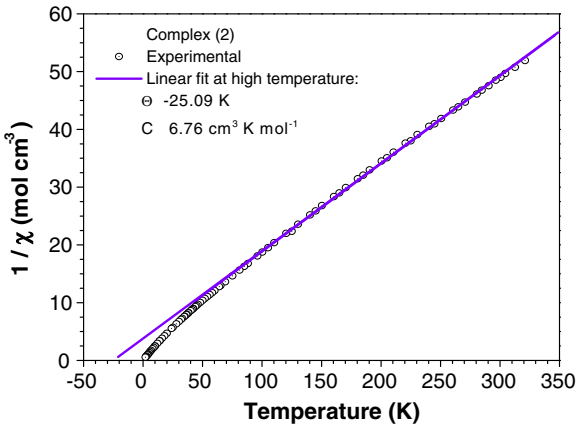

Fig. 4. $1/\chi$ vs. T for **2** (⊙). The solid line represents the best fit to the Curie–Weiss law.

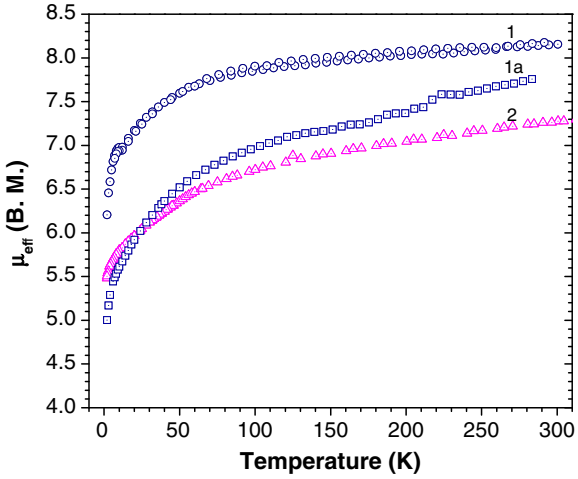

Fig. 5. Experimental μ_{eff} vs. T for **1** (⊙), **1a** (□) and **2** (△).

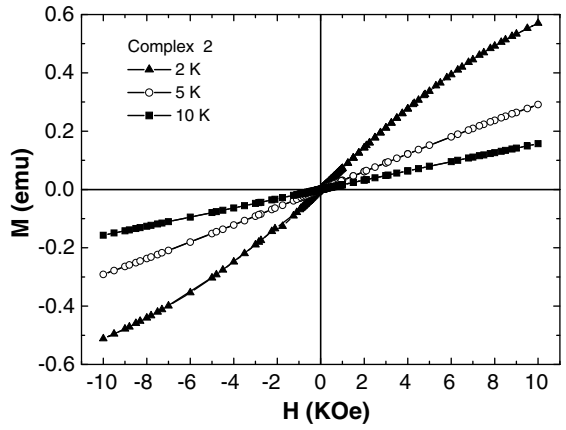

Fig. 6. Isothermal magnetisation of **2** measured in the paramagnetic region at 10 K (■), at 5 K (○) and at 2 K (▲).

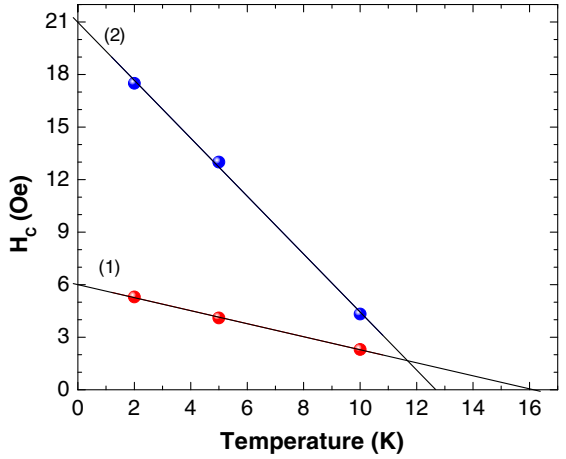

Fig. 7. Coercive field (H_c) versus temperature for compounds **1** and **2**. Accordingly a weak ferromagnetic ordering exist for the two compounds with a Curie temperature about 13 and 16 K.

3.6. X-ray crystallographic studies of *1* and *2*

The binuclear nature of compounds **1** and **2** was confirmed by an X-ray crystallographic study of crystals that were grown from methanol. The most relevant crystallographic data and selected geometric parameters are summarised in Tables 4 and 5.

The asymmetric unit of compound **1** consists of two crystallographically independent molecule halves of $[Co_2(tmpc)Cl_2]^{2+}$ cations both of which are located on inversion centres, and one $[CoCl_4]^{2-}$ anion as counterion. The propylene groups in one of the two molecule halves are so disordered over two positions (occupation factors 0.6 and 0.4) that a total of three different conformers with C_i point group symmetry are present in the unit cell in a 1:0.6:0.4 stoichiometry. Conformer I is shown in Fig. 8 while conformers IIA and IIB are depicted in Fig. 9.

Comparing the coordination geometries of the two independent metal centres in the asymmetric unit, only relatively small variations of the bond lengths and bond angles can be found (Table 5); this might be attributed to the intermolecular packing forces. The geometric parameters are also very similar to that determined for $[Co_2(tmpc)Cl_2][BF_4]_2$, that contains the same cation, with a different anion in the crystal lattice [**4h**]. As can be seen from Figs. 8 and 9, the coordination environments of the penta-coordinate cobalt(II) ions are distorted trigonal bipyramidal, the axial sites being occupied by one pyridine nitrogen and one tertiary nitrogen atom, Co–N4/54 = 2.124(5)/2.136(5) and Co–N2/52 = 2.206(4)/2.231(5) Å, respectively. The equatorial sites are formed by the rest of the pyridine and tertiary nitrogen atoms, Co–N1/51 = 2.098(4)/2.047(5) and Co–N3/53 = 2.159(4)/2.113(5) Å, respectively, and one chlorine atom, Co–Cl1/51 = 2.2697(16)/2.2536(17) Å. It should be noticed that the average axial Co–N bonds are significantly longer than the equatorial Co–N bonds; Δd = 0.058 for the pyridine nitrogen and $\Delta d = 0.083$ Å for the tertiary amine nitrogen atoms.

However, all values are in agreement with the bond lengths observed for other five-coordinate cobalt(II) complexes of the CoN_4Cl-type, 2.051–2.119 for Co–N_{pyr}, 2.121–2.523 for Co–$N_{tetramine}$ and 2.219–2.507 for Co–Cl [18]. The distortion from ideal trigonal bipyramidal geometry can be evaluated on the basis of the axial and equatorial N–Co–N bond angles. The *trans*-oriented N–Co–N

Table 4
Crystallographic data for compounds **1** and **2**

Compound	**1**	**2**
Formula	$C_{34}H_{44}Cl_6Co_3N_8$	$C_{34}H_{44}Co_2N_{12}O_{12} \cdot CH_3OH$
M	954.26	962.71
Crystal system	monoclinic	monoclinic
Space group	$P2_1/c$	$P2_1/n$
a (Å)	13.1701(13)	8.9361(7)
b (Å)	15.9488(15)	21.7157(17)
c (Å)	18.8950(18)	11.5629(9)
β (°)	92.712(2)	104.6920(10)
U (Å^3)	3964.4(7)	2170.5(3)
Z	4	2
D_{calc} (Mg m^{-3})	1.599	1.473
μ (Mo Kα) (mm^{-1})	1.682	0.839
Crystal dimensions (mm)	0.25 × 0.32 × 0.47	0.18 × 0.25 × 0.43
Number of reflections measured	28 169	17 306
Number of independent reflections	6988	3005
Number of observed reflections[a,b]	6041	2519
Number of variables	459	289
Goodness-of-fit	1.258	1.208
R[c]	0.072	0.079
wR[d]	0.139	0.212
$\Delta\rho_{max}$ (e Å^{-3})	0.97	0.77
$\Delta\rho_{min}$ (e Å^{-3})	−0.60	−0.27

[a] $F_o > 4\sigma(F_o)$.
[b] θ limits $2 < \theta < 25$ for **1** and $2 < \theta < 25$ for **2**.
[c] $R = \sum(F_o^2 - F_c^2)/\sum F_o^2$.
[d] $R_w = [\sum w(F_o^2 - F_c^2)^2/\sum w(F_o^2)^2]^{1/2}$.

Table 5
Selected bond lengths (Å), bond angles (°) and torsion angles (°) for compounds **1** and **2**

Compound	**1**[a]		**2**
Bond lengths (Å)			
Co1–N1	2.098(4)/2.047(5)	Co1–N1	2.113(6)
Co1–N2	2.206(4)/2.231(5)	Co1–N2	2.157(5)
Co1–N3	2.159(4)/2.113(5)	Co1–N3	2.217(5)
Co1–N4	2.124(5)/2.136(5)	Co1–N4	2.103(6)
Co1–Cl1	2.2536(17)/ 2.2536(17)	Co1–O1	2.130(5)
		Co1–O2	2.240(5)
Bond angles (°)			
N1–Co1–N2	79.11(16)/82.18(18)	N1–Co1–N2	78.6(2)
N1–Co1–N3	116.51(16)/111.05(19)	N1–Co1–N3	115.12(2)
N1–Co1–N4	91.45(17)/95.65(19)	N1–Co1–N4	94.0(2)
N2–Co1–N3	82.52(16)/83.86(18)	N2–Co1–N3	81.8(2)
N2–Co1–N4	152.68(18)/161.13(19)	N2–Co1–N4	154.0(2)
N3–Co1–N4	78.89(18)/79.43(18)	N3–Co1–N4	79.0(2)
N1–Co1–Cl1	111.26(13)/111.11(15)	N1–Co1–O1	139.1(2)
N2–Co1–Cl1	108.66(12)/104.13(14)	N2–Co1–O1	110.3(2)
N3–Co1–Cl1	132.20(12)/137.77(14)	N3–Co1–O1	105.7(2)
N4–Co1–Cl1	98.66(14)/94.16(14)	N4–Co1–O1	91.7(2)
		N1–Co1–O2	82.2(2)
		N2–Co1–O2	99.8(2)
		N3–Co1–O2	162.4(2)
		N4–Co1–O2	103.8(2)
Torsion angles (°)			
N1–C1–C6–N2	−23.9(7)/−7.7(9)	N1–C1–C6–N2	−21.7(8)
N2–C7–C8–N3	−53.9(6)/56.0(7)	N2–C7–C8–N3	−52.3(8)
N3–C9–C10–N4	−32.6(7)/−34.0(7)	N3–C9–C10–N4	−45.2(7)

[a] Values are given for the two independent molecule halves present in the asymmetric unit of the crystal lattice (conformers I and II). Only the atom numbering for conformer I is given since the numbering sequence for conformers IIA and IIB is analogous (+50).

bond angles formed between the axial substituents are significantly different from 180° and, furthermore, different from each other, N2–Co–N4 = 152.68(18)° and N52–Co51–N54 = 161.13(19)°. Accordingly, the N–Co–N/Cl bond angles in the equatorial plane vary from 111.26(13)° to 132.20(12)° for Co1 and from 111.05(15)° to 137.77(14)° for Co51, whereas the smaller values correspond to the N_{pyr}–Co–Cl and N_{pyr}–Co–$N_{tetramine}$ and the larger values to the $N_{tetramine}$–Co–Cl bond angle. An evaluation of the angular strains generated at the metal centres by the formation of three five-membered chelate rings shows that the strain is smallest for the central *N*,*N*′,*N*″,*N*‴-tetrasubstituted ethylenediamine moiety, N_{pyr}–Co–$N_{tetramine}$ = 79.9(2)° and $N_{tetramine}$–Co–$N_{tetramine}$ = 83.2(2)° (mean values). This observation can be confirmed by the corresponding mean values of the N–C–C–N dihedral angles, which are 24.5(8)° and 55.0(7)°, respectively (Table 5).

As has been already mentioned, the unit cell of compound **1** contains $[Co_2(tmpc)Cl_2]^{2+}$ cations with three different conformations for the central macrocyclic ring. The three conformers can be distinguished most easily by their Co–N–C–C dihedral angles. While for conformer I (Fig. 8) the Newman projections show a counter-clockwise rotation of the C16 carbon in relation to the Co atom, Co1–N2–C15–C16 = 68.8(5)°, for conformers IIA and IIB the corresponding rotations occur in the opposite direction, Co51–N52–C65–C66 = −73.7(2) and Co51–N52–C65B–C66B = −58(3)°. Conformers IIA and IIB can be distinguished by the N–C–C–C dihedral angles; this indicates a *gauche*-configuration for the central C–C bond in the former case, N52–C65–C6–C67 = 86.0(16)° and an approximate *anti*-configuration in the latter case, N52–C65B–C66B–C67 = 150(2)°. According to the refinement realized for the occupation factors of the two conformers, conformer IIA is more highly populated in the crystal lattice than in conformer IIB (60:40). Apart from a difference in thermodynamic stability, this distribution may be affected by intermolecular interactions in the crystal lattice; however, there are only weak C–H···Cl intermolecular interactions.

In contrast to compound **1** the asymmetric unit of compound **2** contains only one crystallographically independent molecule half of the $[Co_2(tmpc)(NO_3)_2]^{2+}$ cation that is also located on an inversion centre. As can be seen from Fig. 10 and Table 5, the cobalt centres in complex **2** have very similar coordination environments when compared to complex **1**, the main difference being the coordination of a nitrate ion instead of the chloride. Since the nitrate ions are coordinated in a bidentate mode, Co–O1 = 2.130(5) and Co–O2 = 2.240(5) Å, the coordination number increases to six; however, the overall coordination geometry resembles the environment found for the penta-coordinate complex **1**. For complex **2** the Co–N distances vary from 2.103(6) to 2.217(5) Å and, in this case there is indeed no significant difference between the axial and equatorial bond lengths, $\Delta d = 0.035$ Å). The N–Co–N bond angle formed between the axial substituents N2–Co–N4 = 154.0(2)° is slightly increased when compared with compound **1**, 152.7(2)°. The latter observations show that in the axial direction the steric bulk of the chloride ion is larger than that of the nitrate group. The conformation found for the central macrocyclic ring in complex **2** is almost identical to that of conformer I in the crystal lattice of **1**.

In the dinuclear complexes described here the *tmpc* ligands adopt an overall chair conformation in which the two metal centres are coordinated *exo* (Scheme 3) [19]. A similar conformation and coordination mode has been reported previously for a related complex with a copper(II) metal centre, $[Cu_2(tmpc)Br_2][ClO_4]$ (**6**). All other dinuclear, five-coordinate complexes that have been characterized by X-ray crystallography so far present a boat conformation in which the two metal centres are bridged by a OH^-, NO_3^-, F^- or Cl^- anion (Scheme 3) [4g,20].

3.7. Electrochemistry

The Co(II) series of *tmpc* complexes display peaks associated with Co(II)/(III) and Co(II)/Co(I) redox processes. In order to establish the independence of

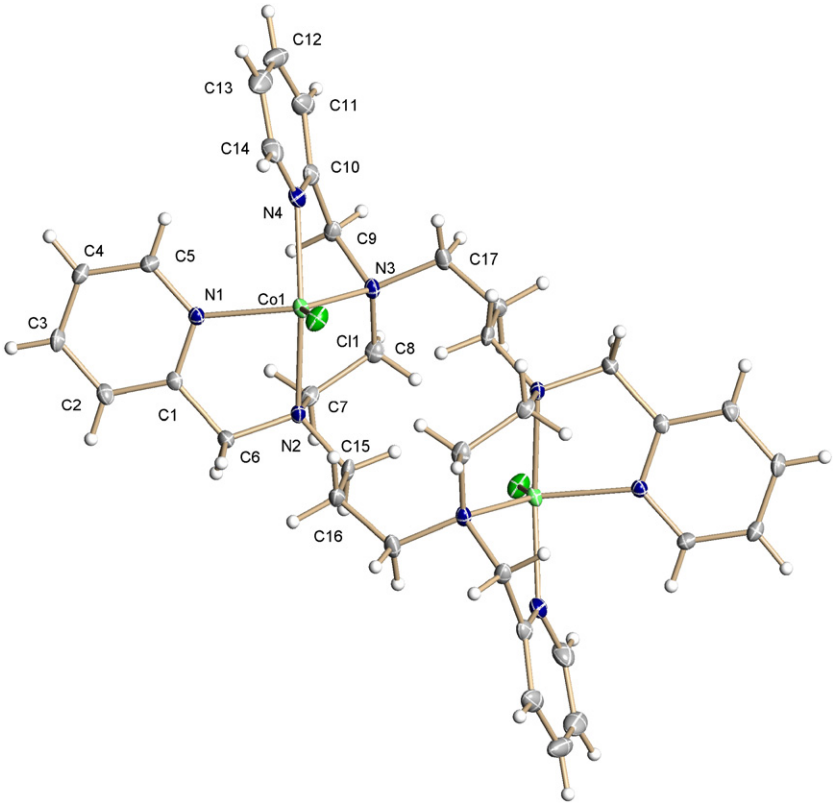

Fig. 8. Perspective view of the molecular structure of the cation of **1** (conformer I).

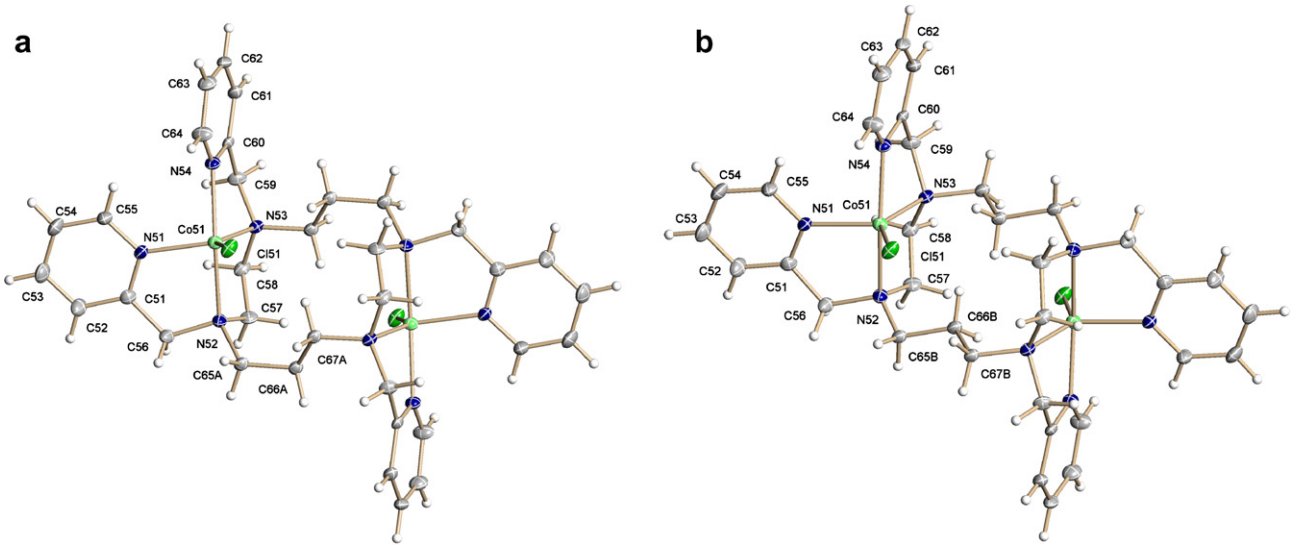

Fig. 9. Perspective view of the molecular structure of the cation of **1** (conformers IIA and IIB).

each oxidation and the reduction signals and the corresponding reverse processes, inversion potential ($E_{+\lambda}$ and $E_{-\lambda}$) studies were carried out in all cases. It is worth mentioning that for the first time these electrochemical measurements were carried out in a suitable media such that they allowed us to open the experimental window and observe a kind of signals that have not been observed before.

3.7.1. *[Co$_2$(tmpc)Cl$_2$][CoCl$_4$] (**1**)*

As can be seen from the reference measurement for the electrolyte solution, there is no electron exchange between the glassy carbon electrode and the electrolyte solution (Bu_4NPF_6/CH_3CN) in the potential range studied. The cyclic voltammograms of [Co$_2$(*tmpc*)Cl$_2$][CoCl$_4$] (**1**) were scanned in both potential directions, positive and negative and these are shown in Fig. 11a and b, respectively. The

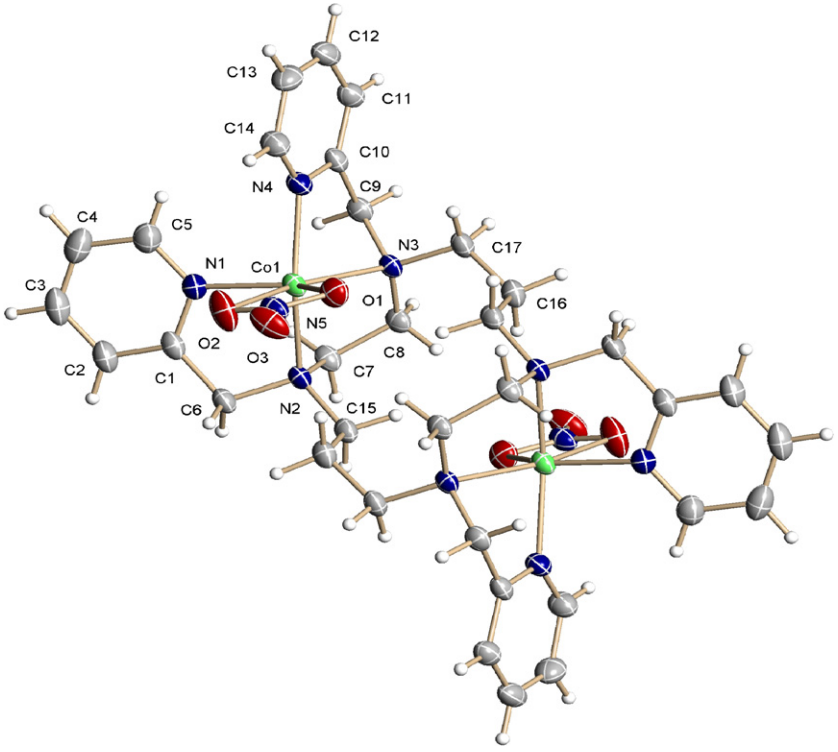

Fig. 10. Perspective view of the molecular structure of the cation of **2**.

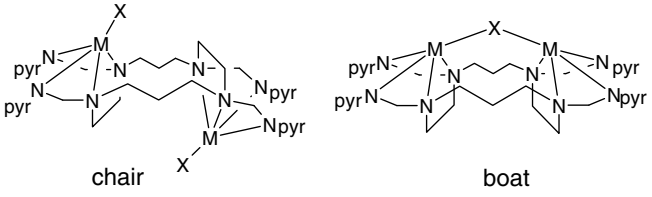

Scheme 3. Conformational isomers of the *tmpc* in the binuclear complexes.

cyclic voltammograms were analysed separately in the anodic and the cathodic region in order to interpret them with no ambiguity.

The anodic region (Fig. 11a) of **1** shows four non-reversible oxidation processes (Ia, IIa, IIIa and IVa) at anodic potential peaks values: $E_{ap} = 0.01$, 0.63, 1.10 and 1.19 V, respectively. In the negative direction, after reaching the inverse anodic potential ($E_{+\lambda} = 1.40$ V), the cyclic voltammogram shows two reduction signals ($IIIc_1$, and $IIIc_2$) at

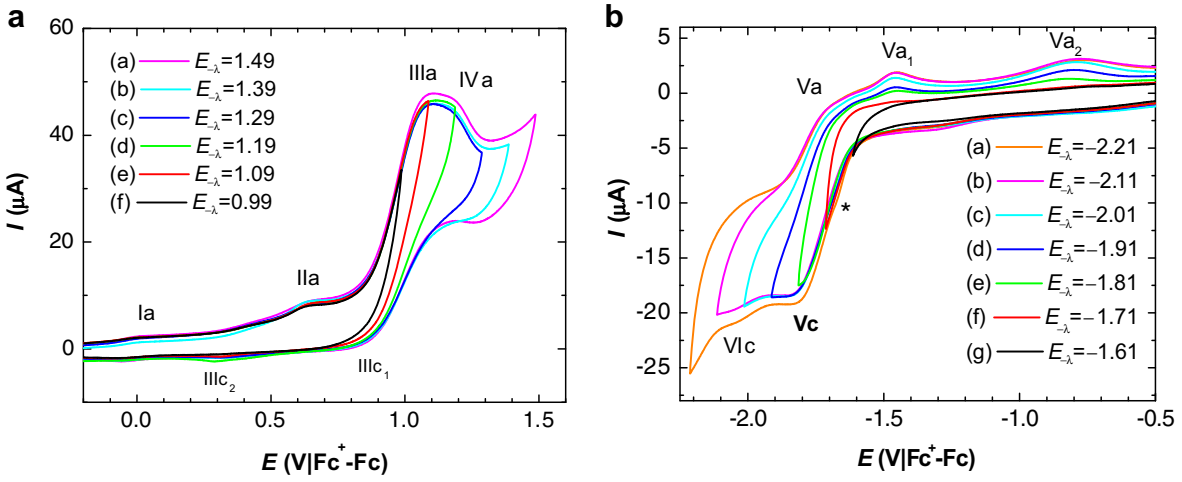

Fig. 11. Cyclic voltammograms of 1 mM of **1** in CH_3CN at 100 mV/s on a GC electrode. Potential scan initiated in (a) the anodic direction from $E_{i=0}$ inverting the scan direction at different ($E_{+\lambda}$) switching potentials and (b) in the cathodic direction from $E_{i=0}$ inverting the scan direction at different ($E_{-\lambda}$) switching potentials.

the cathodic potential peaks $E_{pc} = 0.80$ and 0.29 V, respectively. When a variable inverse anodic potential study was carried out, it was possible to verify that the latter cathodic signals, $IIIc_1$ and $IIIc_2$, correspond to the reduction of the oxidised product in IIIa.

The cathodic region (Fig. 11b) of **1** shows only two signals: Vc and VIc at cathodic potential peak values: $E_{pc} = -1.85$ and -2.40 V, respectively. The first, Vc, is a *quasi* reversible process (Vc/Va at $E_{1/2} = -1.78$ V), while the second, VIc, is not.

The most intense anodic signals IIIa, and the $IIIc_1$ and $IIIc_2$ (Fig. 11a) are very similar to those in the voltammogram of the chloride ion (0.001 M Et_4NCl solution; $E_{ap} = 1.44$ and $E_{cp} = 1.30$ and 0.77 V) obtained under the same conditions. However, a small anodic shift in the potential values of IIIa, $IIIc_1$ and $IIIc_2$ in **1** was observed. This difference can be accounted for the coordination effect in the tetrachlorocobaltate species. Hence, the signals IIIa, $IIIc_1$ and $IIIc_2$ are assigned to the chloride ions coordinated to the tetrachlorocobaltate anion. This electrochemical behavior coincides well with another reported chloride salt [21].

In order to assign the redox potential values of cobalt in the cation with no ambiguity, the hexafluorophosphate derivative (**1a**) was synthesised and its cyclic voltammograms were registered under the same conditions.

3.7.2. $[Co_2(tmpc)Cl_2](PF_6)_2$ (**1a**)

The full cyclic voltammogram of **1a** is displayed in Fig. 12. The anodic region (from -0.20 to 1.70 V) (Fig. 13a) shows a *quasi* reversible system with a half wave potential, $E_{1/2} = 1.00$ V (I′a/I′c). The cathodic region, on the other hand (Fig. 13b), shows several reduction processes and their corresponding oxidation signals, where a *quasi* reversible system V′a/V′c with a half wave potential: $E_{1/2} = -1.71$ V is observed. Therefore, the system I′a/I′c, $E_{1/2} = 1.00$ V is assigned to the Co(III)/Co(II) pair in the cation and the system V′a/V′c to the Co(II)/Co(I).

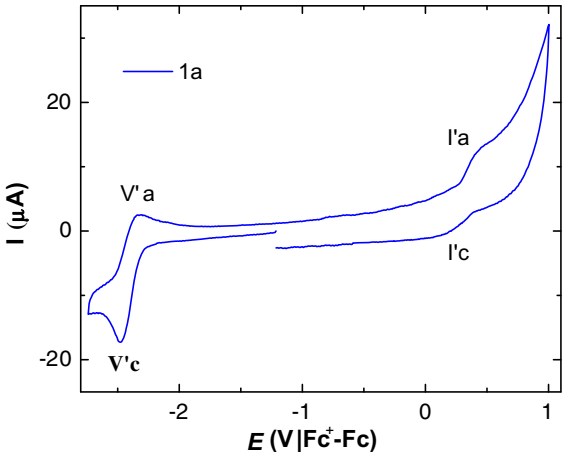

Fig. 12. Cyclic voltammogram of 1 mM of **1a** in CH_3CN at 100 mV/s on a GC electrode. Potential scan initiated in the cathodic direction from $E_{i=0}$ over the full width potential window.

Comparing these voltammograms with those of **1** (Figs. 13a and 11a, respectively), the previous assignation of the signals can be confirmed: IIIa, IVa, $IIIc_1$ and $IIIc_2$ for the oxidation and reduction of the Cl^- of the counterion of **1**, therefore, the signals in the anodic region, I′a/I′c can be assigned unambiguously to the Co(II) → Co(III) redox process. On the other hand, in the cathodic region, V′a/V′c is assigned to the Co(II) → Co(I) redox process. The change of the counterion proved to be very useful since the signals of the chloride interfered with the clear observation of the oxidation and reduction signals of cobalt in the cation.

3.7.3. $[Co_2(tmpc)(NO_3)_2][NO_3]_2 \cdot MeOH$ (**2**)

Fig. 14 shows the voltammogram of **2**. In the anodic region (0.0–2.5 V) an irreversible system is observed with an anodic potential signal, $E_{ap} = 2.07$ V. On the other hand, in the cathodic region several reduction processes and their corresponding oxidation processes are observed.

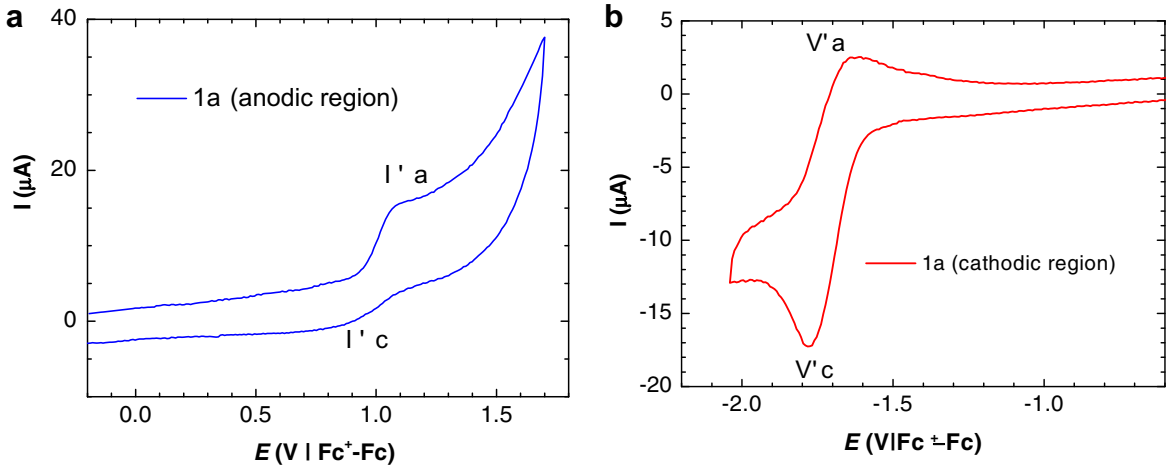

Fig. 13. Cyclic voltammogram of 1 mM of **1a** in CH_3CN at 100 mV/s on a GC electrode. Potential scan initiated in (a) anodic region (-0.2 to 1.7 V/Fc^+–Fc), (b) Cathodic region (-0.2 to 2.1 V/Fc^+–Fc).

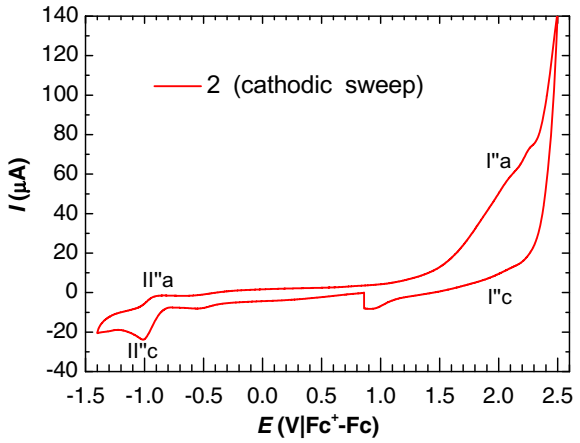

Fig. 14. Cyclic voltammogram of 1 mM of **2** in CH_3CN at 100 mV/s on a GC electrode. Potential scan initiated in the cathodic direction from $E_{i=0}$ over the potential window of −1.4 to 2.5 V/Fc^+–Fc.

From this, the quasi reversible system II″c/II″a has a half wave potential, $E_{1/2} = -0.96$ V. In this case, in the anodic region it is not possible to assign signals unequivocally to the system Co(III)/Co(II) since the signal I″a is very intense and it does not present typical features of reversibility. It is very likely that the coordinated ligand *tmpc* is undergoing an oxidation process. This proposal is based on the observation of the *tmpc*, which resulted electroactive showing an irreversible oxidation process at $E_{ap} = 1.80$ V proceeded by a signal probably due to an adsorption process. The redox potential value difference between these signals in *tmpc* and that observed for **1a** at $E_{ap} = 2.07$ V is attributed to the coordination effect of the ligand *tmpc*. On the other hand, in the cathodic region, the II″a/II″c is assigned to the Co(II)/Co(I) pair in **2**.

In order to establish the effects of the inner coordination sphere of compounds **1**, **1a** and **2** on the Co(II), their voltammograms were compared. Due to the interferences in the anodic region of the $[CoCl_4]^{2-}$counterion and the possible oxidation signals of the coordinated *tmpc*, an analysis of the cathodic region was carried out, particularly in the zone of the signals of Co(II)/Co(I). The voltammograms of **1**, **1a** and **2** are shown in Fig. 15. When the cathodic sweep starts, it can be noticed for **1** and **1a** (Plots **a** and **c**, Fig. 15) that the reduction signals from Co(II) to Co(I), present potential values that are almost identical ($E_{1/2} = -1.01$ V). The signal (*) corresponds to the reduction of Co(II) that is found in the counterion in compound **1**. Again the reduction signals from Co(II) to Co(I) present potential values at ($E_{1/2} = -0.96$ V) in compound **2**, which is interpreted as the coordination environment for Co(II) is slightly less favourable in **2** compared with **1** and **1a**.

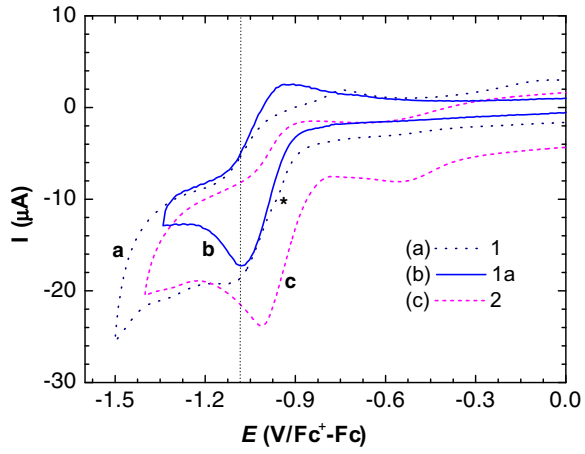

Fig. 15. Cathodic region (0.0 to −1.5 V/Fc^+–Fc) of cyclic voltammograms, obtained at 100 mV/s on a GC electrode, for 1 mM of: (a) **1**, (b) **1a** and (c) **2** solutions in CH_3CN.

4. Summary and conclusions

By using the sterically hindered *tpmc* ligand, three new high spin cobalt(II) complexes $[Co_2(tmpc)Cl_2]CoCl_4$ (**1**), $[Co_2(tmpc)Cl_2][PF_6]_2$ (**1a**) and $[Co_2(tmpc)(NO_3)_2][NO_3]_2 \cdot MeOH$ (**2**) were synthesised and characterised by different techniques. The X-ray crystal structures of **1** and **2** demonstrate that in both complexes the metal ion has *exo*-coordination with the macrocyclic ligand. In compound **1** the Co(II) ions are five coordinated with trigonal bipyramidal geometry but in compound **2** the Co(II) ions are six coordinated with a distorted octahedral geometry. The electronic spectra of **1** and **1a** are very similar reflecting the similarities between the electronic environments of the metals in the trigonal bipyramidal geometry in both complexes, in contrast with **2** which possesses a distorted octahedral geometry. The EPR spectra obtained at 10 K for **1, 1a** and **2** showed the pseudo-rhombic spectra. The magnetic moments, $\mu_{eff} = 8.2$, 7.6 and 7.2 BM at 298 K found for **1**, **1a** and **2** clearly showed the expected *spin–orbit* coupling for high spin, d^7 dinuclear Co(II) complexes. Magnetic measurements show a deviation from the Curie–Weiss law at low temperatures. Two magnetic orderings were observed, at high temperatures, an antiferromagnetic coupling with a Curie–Weiss temperature $\Theta = -9.0$, −20.0 and −25.0 for **1**, **1a** and **2**, respectively, was found, below 20 K a change to a weak ferromagnetic coupling was observed, this explains the deviation of the Curie–Weiss graph at low temperatures. Isothermal magnetic measurements at low temperature show a weak hysteresis which was confirmed by the small coercive field found at low temperature. In addition, the chemical oxidation of **1**, **1a** and **2** did not take place even with strong oxidants, for the first time an explanation for the observation that these cobalt(II) compounds are very stable towards oxidation is offered in terms of their high redox potential values obtained for **1**, **1a**, and **2**. Our electrochemical studies in solution by cyclic voltammetry show very high redox potential values. The electrochemical interpretation of **1** was more complicated because of the presence of chloride ions and a cobalt counteranion. The exchange of the counteranion to hexafluorophosphate helped to confirm the oxidation potential of Co(II) to Co(III) ions in the

coordination sphere ($E_{1/2} = 1.00$ V). The variation of the reduction potential values for Co(II) to Co(I) of **2** from **1** and **1a** indicates that the slight variation in the coordination sphere of **2**. Analysis of the inversion electrochemical studies proved that these complexes are relatively more stable towards its electrochemical reduction. This may be due to the absence of ligand flexibility, the macrocyclic effect and the presence of strong steric hindrance of the pyridine groups. For the first time an explanation to the unusual oxidation property for cobalt(II) is offered in terms of redox potential values.

Acknowledgements

We gratefully acknowledge the financial support of DGAPA-UNAM, research project IN212805, and of CONACYT, research project 41128-Q for the acquisition of an EPR spectrometer and of the USAI (Unidad de Servicios de Apoyo a la Investigación, Facultad de Química) for analytical services. R.E. thanks DGAPA-UNAM for a research project too.

Appendix A. Supplementary material

CCDC 620506 and 620507 contain the supplementary crystallographic data for this paper. These data can be obtained free of charge from The Cambridge Crystallographic Data Centre via www.ccdc.cam.ac.uk/data_request/cif. Supplementary data associated with this article can be found, in the online version, at doi:10.1016/j.ica.2008.01.049.

References

[1] C.M. Che, W.T. Tang, T.C.W. Mak, J. Chem. Soc., Dalton Trans. (1988) 2879.
[2] (a) D. Meyerstein, Coord. Chem. Rev. 141 (1999) 185;
(b) M.A. Masood, D.J. Hodgson, Inorg. Chem. 33 (1994) 2488;
(c) X.H. Bu, X.C. Cao, W.Q. Zhang, R.H. Zhang, Transition Met. Chem. 22 (1997) 513.
[3] (a) I. Murase, M. Mikuriya, H. Sonoda, Y. Fukuda, S. Kida, J. Chem. Soc., Dalton Trans. (1986) 953;
(b) M. Mikuriya, S. Kida, T. Kohzuma, I. Murase, Bull. Chem. Soc. Jpn. 61 (1988) 2666;
(c) I. Murase, G. Vuckovic, M. Kodera, H. Harada, N. Matsumoto, S. Kida, Inorg. Chem. 30 (1991) 728;
(d) E. Asato, S. Kida, I. Murase, Inorg. Chem. 28 (1989) 800;
(e) S.G. Kang, S.J. Kim, J.H. Jeong, Polyhedron 17 (1998) 3227.
[4] (a) G. Vuckovic, V. Stanic, S.P. Sovilj, M.A. Nikolic, J. Mrozinski, J. Serb. Chem. Soc. 70 (2005) 1121;
(b) H. Harada, M. Kodera, G. Vuckovic, N. Matsumoto, S. Kida, Inorg. Chem. 30 (1991) 1190;
(c) G. Vuckovic, D. Opsenica, S.P. Sovilj, D. Poleti, J. Coord. Chem. 47 (1999) 331;
(d) S.P. Sovilj, G. Vuckovic, K.B. Babc'-Samardzija, N. Matsumoto, V.M. Jovanovic, J. Mrozin'ski, Synth. React. Inorg. Met.-Org. Chem 29 (1999) 785;
(e) Z.M. Miodragovi, G. Vuckovic, V.M. Leovac, V.M. Buzash, Synth. React. Inorg. Met.-Org. Chem 30 (2000) 57;
(f) G. Vuckovic, E. Asato, N. Matsumoto, S. Kida, Inorg. Chim. Acta 171 (1990) 45;
(g) E. Asato, H. Toftlund, S. Kida, M. Mikuriya, K.S. Murray, Inorg. Chim. Acta 165 (1989) 207;
(h) G. Vuckovic, S.B. Tanaskovic, U. Rychlewska, D.D. Radanovic, J. Mrozinski, M. Korabik, J. Mol. Struct. 827 (2007) 80.
[5] J. Narayanan, M.E. Sosa-Torres, R.A. Toscano, J. Chem. Crystallogr. 31 (2001) 129.
[6] N.W. Alcock, K.P. Balakrishnan, P. Moore, J. Chem. Soc., Dalton Trans. (1986) 1743.
[7] Bruker Analytical X-ray Systems, SMART: Bruker Molecular Analysis Research Tool, vol. 5, 2000, p. 618.
[8] Bruker Analytical X-ray Systems, SAINT+NT Version 6.0, 2001.
[9] Bruker Analytical X ray Systems, SHELXTL-NT Version 6.10, 2000.
[10] K. Nakamoto, Infrared and Raman Spectra of Inorganic and Coordination Compounds, 5th ed., John Wiley and Sons, New York, 1997.
[11] F.M. Ramírez, M.E. Sosa-Torres, R. Escudero, J. Padilla, J.A. Ascencio, J. Coord. Chem. 50 (2000) 1.
[12] F.M. Ramírez, M.E. Sosa-Torres, M. Castro, E. Basurto-Uribe, R. Zamorano-Ulloa, F. Del Río-Portilla, J. Coord. Chem. 41 (1997) 303.
[13] A.B.P. Lever, Inorganic Electronic Spectroscopy, 2nd ed., Elsevier Science Publishers Company Inc., New York, 1984, p. 491.
[14] J.R. Pilbrow, Transition Ion Electron Paramagnetic Resonance, Clarendon Press, Oxford, 1990.
[15] O. Kahn, Molecular Magnetism, VCH, Weinheim, 1993.
[16] M. Arnold, D.A. Brown, O. Deeg, W. Errington, W. Haase, K. Herlihy, T.J. Kemp, H. Nimir, R. Werner, Inorg. Chem. 37 (1998) 2920.
[17] (a) M.E. Lines, Phys. Rev. 131 (1963) 546;
(b) B.N. Figgis, M. Gerloch, J. Lewis, F.E. Mabbs, G.A. Webb, J. Chem. Soc. A (1968) 2086;
(c) H. Sakiyama, Inorg. Chim. Acta 359 (2006) 2097.
[18] The CSD System: (a) F.H. Allen, Acta Crystallogr., Sect. B 58 (2002) 380;
(b) I.J. Bruno, J.C. Cole, P.R. Edington, M. Kessler, C.F. Macrae, P. McCabe, J. Pearson, R. Taylor, Acta Crystallogr., Sect. B 58 (2002) 389;
(c) N.A. Bailey, E.D. McKenzie, J.M. Worthington, J. Chem. Soc., Dalton Trans. (1977) 763;
(d) T. Sakurai, K. Kobayashi, A. Hasegawe, S. Tsuboyama, K. Tsuboyama, Acta Crystallogr., Sect. B 38 (1982) 107;
(e) C.M. Che, S.T. Mak, T.C.W. Mak, Inorg. Chem. 25 (1986) 4705;
(f) S. Tsuboyama, J. Fujimoto, S. Hanabira, N. Yasuda, K. Kobayashi, T. Sakurai, K. Tsuboyama, J. Chem. Soc., Dalton Trans. (1996) 45;
(g) M.S. Lah, M. Moon, Bull. Korean Chem. Soc. 18 (1997) 406;
(h) P. Planinic, D. Matkovic-Calogovic, H. Meider, J. Chem. Soc., Dalton Trans. (1997) 3445;
(i) M. Du, Z.L. Shang, Q. Xu, R.H. Zhang, X.B. Leng, X.H. Bu, Acta Crystallogr., Sect. C 56 (2000) 769;
(j) L. Broge, U. Pretzmann, N. Jensen, I. Sotofte, C.E. Olsen, J. Springborg, Inorg. Chem. 40 (2001) 2323;
(k) J.W. Lim, M. Mikuriya, H. Sakiyama, Bull Chem. Soc. Jpn. 74 (2001) 2131;
(l) K. Kreischer, J. Kipke, M. Bauerfeind, J. Sundemeyer, Z. Anorg, Allg. Chem. 627 (2001) 1023;
(m) M. Du, Z.L. Shang, X.B. Leng, X.H. Bu, Polyhedron 20 (2001) 3065;
(n) G.J.P. Britovsek, V.C. Gibson, S.K. Spitzmesser, K.P. Tellmann, A.J.P. White, D.J. Williams, J. Chem. Soc., Dalton Trans. (2002) 1159.
[19] G. Vuckovic, D. Opsenica, S.P. Sovilj, D. Poleti, M. Avramov-Ivic, J. Coord. Chem. 42 (1997) 241.
[20] G. Vuckovic, E. Asato, N. Matsumoto, S. Kida, Inorg. Chim. Acta 171 (1990) 45.
[21] L.A. Ortiz-Frade, L. Ruiz-Ramirez, I. González, A. Marín-Becerra, M. Alcarazo, J.G. Alvarado-Rodríguez, R. Moreno-Esparza, Inorg. Chem. 42 (2003) 1825.